Compressed Edge Spectrum Sensing for Wideband Cognitive Radios

Edgar Beck, Carsten Bockelmann and Armin Dekorsy
Department of Communications Engineering
University of Bremen, Bremen, Germany
Email: {beck, bockelmann, dekorsy}@ant.uni-bremen.de

***Abstract*—Free licensed spectral bands have become rare due to the increasing number of wireless users and their demand for high data rates. Likewise, the static allocation of these bands results in an under-utilization of the spectrum. Cognitive Radio (CR) has emerged as a promising solution to the dilemma by allowing opportunistic users to transmit in the absence of licensed users. Spectrum sensing is therefore the key component of CR and coexistence management in general. In order to detect as much transmission opportunities as possible, a large bandwidth has to be monitored which according to Shannon-Nyquist necessitates high sampling rates. For fast and accurate spectrum estimation, we propose a novel approach called Compressed Edge Spectrum Sensing (CESS) which exploits the sparsity of power spectrum edges and allows for sampling down to 6% of Nyquist without losses in the detection accuracy of occupied and unoccupied spectrum regions.**

I. Introduction

The number of devices with a need for higher data rates is growing due to the transition from voice-only to multimedia-type applications [1]. The concept of Cognitive Radio (CR) [2] has evolved as a result of the ever-increasing demand for new spectral bands and the under-utilization of those already statically allocated. Herein, secondary users are allowed to use vacant bands in the absence of licensed primary users. Similar, Coexistence Management (CM) [3] for Industry 4.0 applications should enable coordination of several wireless connected systems in crowded industrial environments. Therefore, a crucial aspect of CR and CM is spectrum sensing to detect these opportunities for transmission, the so-called white spaces. In order to find as much white spaces as possible and to enhance throughput, a wideband must be sensed with the result of high Nyquist rates. Otherwise, a bank of tunable narrowband bandpass filters, to search one narrowband at a time, would become necessary, which means a considerable implementation challenge and results in a high power consumption not favored in wireless devices. Fortunately, several measurements have shown the spectrum to be under-utilized [1] so that it can be assumed sparse. Therefore, Compressed Sensing (CS) is often mentioned as a way of reducing the load [4], [5], [6]. However, two problems result. On the one hand, CS algorithms add processing complexity and delay. Since the time for detecting sudden interference to a primary user has to be as low as possible, algorithms have to be chosen that can be executed very fast. On the other hand, the Power Spectral Density (PSD) may not always be sparse but crowded, e.g., in a busy environment, which makes application of CS difficult and requires representation in another basis. Because many spectra in practical applications like those of OFDM transmissions exhibit sharp boundaries and can be approximated as piecewise flat, the derivative has a few non-zero elements which depict edges. Thus, it seems reasonable to use the edge spectrum as the sparsity basis which we exploit in this paper. In the following, the underlying theory is described and extended to build a whole processing chain which is able of seeking and classifying occupied and free frequency bands.

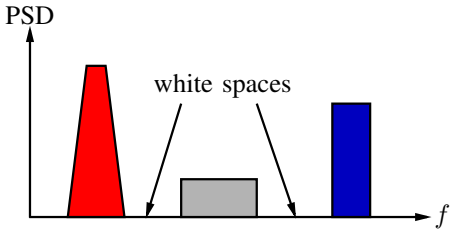

Fig. 1. Sparse spectrum with white spaces.

II. System Model and Problem Statement

Usually, the Nyquist rate equaling the bandwidth of interest is chosen and N samples $\mathbf{x} \in \mathbb{C}^{N\times 1}$ of the continuous signal $x(t)$ are obtained in order to perform spectrum sensing. The signal consists of the several transmissions $\mathbf{x} = \sum_i \mathbf{x}_i$ with a piecewise flat PSD of height σ_i^2 as illustrated in Fig. 1. The transmissions have to be detected and are additionally supposed to be zero-mean wide-sense stationary. These assumptions are valid for many signals appearing in real world settings, e.g., OFDM transmissions [4], since well-defined spectrum masks are employed. To introduce CS, we consider a subsampling approach. It is represented by the subsampling matrix $\mathbf{V} \in \mathbb{C}^{M\times N}$ and generates compressed measurements $\mathbf{y} \in \mathbb{C}^{M\times 1}$. Relating the measurements to the amplitude spectrum $\mathbf{c}$ through

$$\mathbf{y} = \mathbf{V}\mathbf{x} = \mathbf{V}\mathbf{F}^{-1}\mathbf{c} = \mathbf{A}\mathbf{c} \tag{1}$$

with $\mathbf{F} \in \mathbb{C}^{N\times N}$ being the DFT matrix, we formulate the CS reconstruction problem

$$\hat{\mathbf{c}} = \arg\min_{\mathbf{c}} \|\mathbf{c}\|_0 \quad \text{s.t.} \quad \mathbf{y} = \mathbf{A}\mathbf{c} \tag{2}$$

ISBN 978-90-827970-1-5

to find $\mathbf{c}$ with under-determined $\mathbf{A}$ assuming sparsity in $\mathbf{c}$. Here, $\|\mathbf{c}\|_0$ counts the number of non-zero elements in $\mathbf{c}$.

A. Power Spectrum Sensing

To reconstruct the PSD instead of the amplitude spectrum, we make use of the autocorrelation matrix [5]:

$$\mathbf{R_y} = \mathbb{E}\left[\mathbf{y}\mathbf{y}^H\right] = \mathbb{E}\left[\mathbf{A}\mathbf{c}(\mathbf{A}\mathbf{c})^H\right] = \mathbf{A}\mathbf{R_c}\mathbf{A}^H. \quad (3)$$

By definition [5], $\mathbf{s} = \mathbb{E}\left[|\mathbf{c}|^2\right]$ holds so that we can find the entries of $\mathbf{s}$ on the diagonal of $\mathbf{R_c}$. Owing to the wide-sense stationarity of all signals, $\mathbf{R_c}$ is a diagonal matrix. After vectorization and exploitation of the diagonal structure, the following relation can be obtained according to [5]:

$$\mathrm{vec}\left(\mathbf{R_y}\right) = \left(\mathbf{A}^* \otimes \mathbf{A}\right)\mathrm{vec}\left(\mathbf{R_c}\right) = \left(\mathbf{A}^* \odot \mathbf{A}\right)\mathbf{s} = \mathbf{\Phi}\mathbf{s}. \quad (4)$$

Here, $\mathbf{A}^*$ denotes the complex conjugate of $\mathbf{A}$, $\otimes$ the Kronecker product and $\odot$ the column-wise Kronecker product, also known as "Khatri-Rao product". The new PSD sensing matrix $\mathbf{\Phi}$ has the dimensions $M^2 \times N$ and (4) may thus exhibit a unique solution for $M^2 \geq N$. However, the minimum number of measurements required to solve (4) uniquely is derived in [5] and equals $M > N/2$ due to the specific problem structure. In fact, this allows for subsampling without assuming sparsity and solving the overdetermined equation system where $\mathbf{r_y} = \mathrm{vec}\left(\mathbf{R_y}\right)$ with the Least Squares (LS) method:

$$\hat{\mathbf{s}} = \arg\min_{\mathbf{s}} \|\mathbf{r_y} - \mathbf{\Phi}\mathbf{s}\|_2^2 \quad \Rightarrow \quad \hat{\mathbf{s}} = \mathbf{\Phi}^{\dagger}\mathbf{r_y}. \quad (5)$$

$\dagger$ indicates the Moore-Penrose pseudoinverse and enables solutions also for underdetermined equation systems which can be treated as l_2-approximations of the l_0-norm in the equivalent CS reconstruction problem. This problem can be stated as

$$\hat{\mathbf{s}} = \arg\min_{\mathbf{s}} \|\mathbf{s}\|_0 \quad \text{s.t.} \quad \mathbf{r_y} = \mathbf{\Phi}\mathbf{s} \quad (6)$$

and allows for further subsampling since it can be solved uniquely for $M > \|\mathbf{s}\|_0$ as derived in [5]. In other words, a minimum average sampling rate equaling the actual occupied bandwidth becomes necessary lowering the requirements in a practical implementation. The compression ratio reads $\kappa = M/N > \|\mathbf{s}\|_0/N$. This means a reduction of 50% compared to (2) and is due to the assumptions made about stationarity. For the previous bounds to be valid, $\mathbf{A}$ has to be full spark.

B. Practical Considerations

In a practical implementation, solving (6) requires Q measurements $\mathbf{y}_i$ to approximate the expected value of the autocorrelation by the mean where high values of Q lead to a high noise or error reduction:

$$\hat{\mathbf{R}}_{\mathbf{y}} = \frac{1}{Q}\sum_{i=1}^{Q}\mathbf{y}_i\mathbf{y}_i^H. \quad (7)$$

These measurements are obtained in a time window of length Δt assuming wide-sense stationarity as illustrated in Fig. 2. It

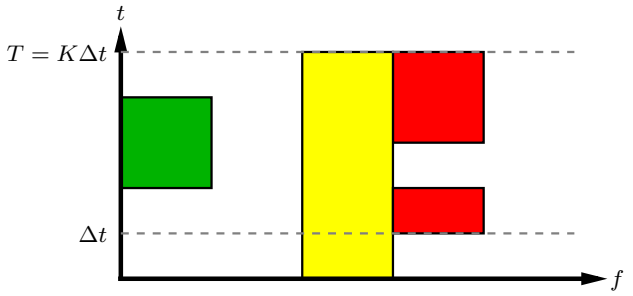

Fig. 2. Occupation of a spectrum in time t and frequency f. The spectrum is assumed stationary in one time window Δt equaling the time resolution.

shows the varying occupation of spectrum which remains constant in one time window. If T_{S} denotes the Nyquist sampling period and N the frequency resolution, the whole sampling time for (7) amounts to $\Delta t = QNT_{\mathrm{S}}$. Therefore, a trade-off between fast detection, resolution and noise suppression has to be considered. Because noise is present in practical settings, (6) has to be modified to include a bounded error ϵ of the ℓ_2-norm:

$$\hat{\mathbf{s}} = \arg\min_{\mathbf{s}} \|\mathbf{s}\|_0 \quad \text{s.t.} \quad \|\mathbf{r_y} - \mathbf{\Phi}\mathbf{s}\|_2 \leq \epsilon. \quad (8)$$

III. Compressed Edge Spectrum Sensing

A. One-dimensional Edge Spectrum Sensing

Unfortunately, there is no guarantee for the spectrum to be sparse since it can be crowded or full in worst case. One solution to overcome this problem is to consider the edges $\mathbf{z}$ of the piecewise constant spectrum due to the fact that there are considerably fewer edges (exactly J) than occupied entries of the PSD and entries in general ($J = \|\mathbf{z}\|_0 \leq \|\mathbf{s}\|_0 \ll N$). The definition of a new CS problem where the power spectrum in (4) is replaced by the edge spectrum immediately suggests itself. Both are related to each other through a numerical derivation

$$\mathbf{s} = \mathbf{\Gamma}^{-1}\mathbf{z}, \quad (9)$$

with $\mathbf{\Gamma} \in \mathbb{C}^{N\times N}$ being the difference matrix

$$\mathbf{\Gamma} = \begin{bmatrix} 1 & 0 & \dots & 0 \\ -1 & 1 & \ddots & 0 \\ 0 & \ddots & \ddots & \\ 0 & \dots & -1 & 1 \end{bmatrix}. \quad (10)$$

This leads to the CS problem

$$\hat{\mathbf{z}} = \arg\min_{\mathbf{z}} \|\mathbf{z}\|_0 \quad \text{s.t.} \quad \mathbf{r_y} = \left(\mathbf{\Phi}\mathbf{\Gamma}^{-1}\right)\mathbf{z} \quad (11)$$

defining a new approach that combines the ideas of [4] and [5]. In the following, we designate this approach one-dimensional Compressed Edge Spectrum Sensing (1D CESS). It allows unique reconstruction of the edge spectrum for compression ratios up to $\kappa = M/N > J/N$ which is a result of the fact that the new sensing matrix $\mathbf{\Phi}\mathbf{\Gamma}^{-1}$ has the same spark as the old one. Just the mapping to the null space changes, but not

ISBN 978-90-827970-1-5

the properties of the problem itself. One problem occurring now is that the inverse $\mathbf{\Gamma}^{-1}$ is a summation matrix summing up a certain amount of entries of the respective rows of $\mathbf{\Phi}$. In every j-th column of $\mathbf{\Phi}\mathbf{\Gamma}^{-1}$, $N-j$ columns $\boldsymbol{\phi}_i$ of $\mathbf{\Phi}$ are summed up: $\sum_{i=j}^{N}\boldsymbol{\phi}_i$. Therefore, the coherence should increase significantly which suggests that the CS problem (11) is in contrast to (6) not robust against noise. This indicates that the Restricted Isometry Property (RIP) is just fulfilled barely.

B. Two-dimensional Edge Spectrum Sensing

So far, only edges in the frequency domain have been exploited. But the spectrum also exhibits edges in the time domain as depicted in Fig. 2. This stems from the fact that communication systems are only active for a limited time to adhere to regulation or because of intermittent activity. Hence, this additional structure can be used to create an advanced spectrum sensing algorithm based on the Total Variation Norm (TVN) in two dimensions. For this purpose, K equations from (11) obtained in time windows of length Δt with subsampling matrices $\mathbf{\Phi}_i$ are stacked together into one equation system:

$$\mathbf{r}_T = \begin{bmatrix} \mathbf{r}_{\mathbf{y}_1} \\ \mathbf{r}_{\mathbf{y}_2} \\ \vdots \\ \mathbf{r}_{\mathbf{y}_K} \end{bmatrix} = \begin{bmatrix} \mathbf{\Phi}_1 & \mathbf{0} & \dots & \mathbf{0} \\ \mathbf{0} & \mathbf{\Phi}_2 & \ddots & \vdots \\ \vdots & \ddots & \ddots & \mathbf{0} \\ \mathbf{0} & \dots & \mathbf{0} & \mathbf{\Phi}_K \end{bmatrix} \cdot \begin{bmatrix} \mathbf{s}_1 \\ \mathbf{s}_2 \\ \vdots \\ \mathbf{s}_K \end{bmatrix} = \mathbf{\Phi}_T \cdot \mathbf{s}_T. \tag{12}$$

For maximum sampling efficiency, the sampling process in a practical CS system should be designed to include randomness [7]. Hence, the $\mathbf{\Phi}_i$ are different from each other so that additional information can be used. In order to reconstruct the edges in the time and frequency domain, the 2D-derivative of $\mathbf{s}_T$ has to be minimized which leads to the following TVN minimization problem:

$$\hat{\mathbf{s}}_T = \arg\min_{\mathbf{s}_T} \left\| \mathbf{\Gamma}_{\text{2D}} \mathbf{s}_T \right\|_1 \quad \text{s.t.} \quad \mathbf{r}_T = \mathbf{\Phi}_T \mathbf{s}_T. \tag{13}$$

The 2D-difference matrix $\mathbf{\Gamma}_{\text{2D}} = [\mathbf{\Gamma}_f, \mathbf{\Gamma}_t]^T$ consists of the difference operation in the frequency domain $\mathbf{\Gamma}_f = \mathbf{I}_K \otimes \mathbf{\Gamma}_1$, with $\mathbf{\Gamma}_1 \in \{-1, 0, 1\}^{N-1 \times N}$ denoting

$$\mathbf{\Gamma}_1 = \begin{bmatrix} -1 & 1 & 0 & \dots & 0 \\ 0 & \ddots & \ddots & \ddots & \vdots \\ \vdots & \ddots & \ddots & \ddots & 0 \\ 0 & \dots & 0 & -1 & 1 \end{bmatrix} \tag{14}$$

and $\mathbf{I}_K \in \{0, 1\}^{K \times K}$ the identity matrix, and the difference operation in the time domain $\mathbf{\Gamma}_t \in \{-1, 0, 1\}^{(K-1)N \times KN}$:

$$\mathbf{\Gamma}_t = \begin{bmatrix} -1_{1,1} & 0 & \dots & 0 \\ 0 & -1_{2,2} & \dots & 0 \\ \vdots & \vdots & \ddots & \vdots \\ 1_{N+1,1} & 0 & \dots & -1_{(K-1)N,(K-1)N} \\ 0 & 1_{N+2,2} & \dots & 0 \\ \vdots & \vdots & \ddots & \vdots \\ 0 & 0 & \dots & 1_{KN,(K-1)N} \end{bmatrix}^T. \tag{15}$$

From here on, this algorithm will be denoted as 2D CESS. The motivation for applying it is simple: The necessary minimum number of measurements should intuitively decrease when considering piecewise-constant spectra as depicted in Fig. 2 since more information is exploited. In comparison to the one-dimensional case, the results are expected to allow for greater compression and performance, respectively. But this should happen at the cost of a delay $T = K\Delta t$, the time for collecting the samples.

IV. Processing Chain

Fig. 3 shows the whole proposed processing chain to perform spectrum sensing. First, the signals arrive through a mitigating channel $\mathbf{H}$ and are superimposed with AWGN. After subsampling, the power spectrum $\mathbf{s}$ is reconstructed according to (5), (6), (11) and (13), respectively. Now, the question has to be asked where the bands are located and whether they are occupied or not. Therefore, we apply a simple feature detection. It consists of the Wavelet Edge Detector (WED) and the Energy Detector (ED) [1], [4].

First, the WED detects the band boundaries $\hat{f}_i$ by looking for the local maxima in the derivative $\mathbf{z}$. We notice that direct reconstruction of edges with CESS should make this step redundant since boundaries are expected to be where the derivative is non-zero. However, CS reconstruction as well as spectrum shapes are not perfect and noise makes it impossible to find the true solution. To suppress noise induced edges, we thus additionally apply a thresholding operation. For the sake of simplicity, we do not apply a Gaussian kernel on the PSD or use it even in the reconstruction step, in contrast to [4]. In order to choose a reasonable threshold η_{WED}, its relation to detection and false alarm rates has to be derived:

To begin with, we model the amplitude spectrum as a multivariate complex gaussian random vector $\mathbf{c} \sim \mathcal{CN}(\mathbf{0}, \mathbf{\Sigma})$ with covariance matrix $\mathbf{\Sigma}$. Here, $\mathbf{\Sigma} = \operatorname{diag}\{\dots, \mathbf{\Sigma}_i, \dots\} + \sigma_{\text{n}}^2 \mathbf{I}_N$ is a block diagonal matrix where each band transmission is represented by its power level $\mathbf{\Sigma}_i = \sigma_i^2 \mathbf{I}_{B_i}$ and bandwidth B_i with $\sum_i B_i = N$. Some bands are empty ($\sigma_i^2 = 0$) and consist only of the noise level σ_{n}^2. So the received Nyquist-sampled signal $\mathbf{x}$ consists of additive correlated Gaussian noise. According to (3) and (7), the average of the squared absolute values of $\mathbf{c}$ is the approximated estimate of the power spectrum. For $Q = 1$, one point is distributed according to the chi-square distribution χ_2^2 with two degrees of freedom and variance $(\sigma_i^2 + \sigma_{\text{n}}^2)^2$. If more realizations are examined, the variance decreases by the number of frames Q. Additionally, this results in convergence to a normal distribution according to the central limit theorem. After numerical derivation, the variance $\operatorname{Var}[Z]$ of one point in the edge spectrum $\mathbf{z}$ is the sum of two neighboring variances in the PSD. Hence, the rate

$$P_{\text{F,WED}} = 2 \cdot F_{\mathcal{N}}\left(-\eta_{\text{WED}} / \sqrt{\operatorname{Var}[Z]} \right) \tag{16}$$

for exceeding an absolute value η_{WED} can be stated, with $F_{\mathcal{N}}$ denoting the cumulative function of the standard normal distribution. In order to generate a threshold satisfying a false alarm rate $P_{\text{F,WED}}$, we invert the equation. We choose

ISBN 978-90-827970-1-5

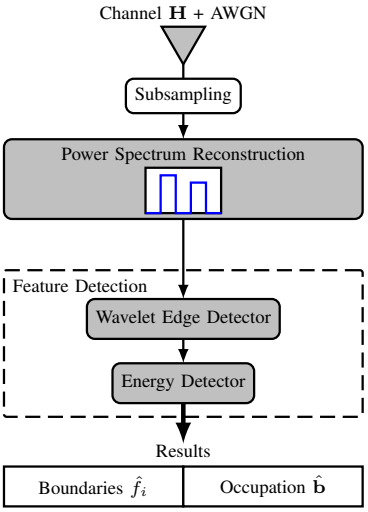

Fig. 3. Proposed design of the spectral estimator.

TABLE I
DEFAULT SIMULATION PARAMETER SET.

parameter	N	Q	κ	β	σ_n^2	$P_\mathrm{F,WED}$
value	100	1000	0.06	0.4	0.1	0.1%

the part of the spectrum with highest signal power σ_i^2 for calculating the variance $\mathrm{Var}[Z] = 2\left(\sigma_i^2+\sigma_\mathrm{n}^2\right)^2/Q$ of the random variable since we have to cover the worst case. Analogously, the missed detection rate

$$P_\mathrm{MD,WED} = F_\mathcal{N}\left(\frac{\eta_\mathrm{WED}-\mu}{\sqrt{\mathrm{Var}[Z]}}\right) - F_\mathcal{N}\left(\frac{-\eta_\mathrm{WED}-\mu}{\sqrt{\mathrm{Var}[Z]}}\right) \quad (17)$$

at one noise-signal edge with variance $\mathrm{Var}[Z] = \sigma_\mathrm{n}^4/Q + \left(\sigma_i^2+\sigma_\mathrm{n}^2\right)^2/Q$ and height $\mu = \sigma_i^2 - \sigma_\mathrm{n}^2$ can be derived.

In the last step, the energy detector similarly compares the average carrier amplitude between two boundaries to a threshold depending on the noise level. In contrast to literature [1], [8], we choose it to be the same except for the noise level that was not considered at the WED stage and has to be added: $\eta_\mathrm{ED} = \eta_\mathrm{WED} + \sigma_\mathrm{n}^2$. This is reasonable since the height of rectangular shapes corresponds to the height of the respective edges. Because the spectrum is expected not to be fully occupied, the noise floor can be extracted from a band with the lowest energy which was done in the simulations. In the end, one receives the binary vector $\hat{\mathbf{b}}$ comprised of the information regarding occupation in every single band.

V. Simulation Results

A. Test Setup

To evaluate CESS, we assumed allocation of the 2.45GHz-ISM-band in accordance with the 802.11g/n-standard. In addition, we added a fifth band at 90 MHz to those at 10, 30, 50 and 70 MHz to enable full occupation of a spectrum with 100 MHz bandwidth. Signals were modeled as lowpass-filtered AWGN as before, with a bandwidth of 20 MHz and carrier power

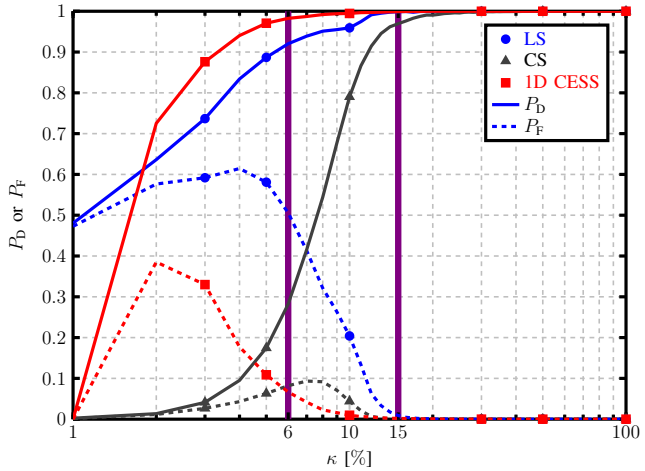

Fig. 4. Detection and false alarm rates of 1D CESS in comparison to LS and CS reconstruction for various compression κ.

$\sigma_i^2 \in \{4,6,8,10,12\}$. We fixed occupation $\beta = \|\mathbf{s}\|_0/N$, and thus the number of signals, to maintain the same condition and modulated them to a randomly selected carrier. For investigation of 2D CESS, also time behavior had to be modeled. Hence, a Markov model with the states empty and occupied was defined for every single band with the same mean and starting occupation β. Here, the probability for changing the state after one time slot Δt from empty to occupied was set to $1/30$ and $1/20$ vice versa. For CS reconstruction, we used the OMP (Orthogonal Matching Pursuit) algorithm, and for TVN minimization, the convex optimization toolbox CVX [9] with the solver SDPT3. In both cases, we chose the stopping criterion to be the true residual $\epsilon = \|\mathbf{R_y} - \hat{\mathbf{R}}_\mathbf{y}\|_F$ calculated with the ideal spectrum shape in order to show the best theoretical performance. In practice, other criteria have to be used. Table I shows the default simulation parameters reflecting practical settings. An appropriate threshold η_WED to realize a sufficient dynamic range for the test signals can be obtained by dynamically estimating $\hat{\mathrm{Var}}[Z] = 2\cdot\max(\hat{\mathbf{s}})^2/Q$ and choosing $P_\mathrm{F,WED} = 0.1\%$. To fulfill null space criterion and RIP with high probability, the subsampling matrix $\mathbf{V}$ was set to a Gaussian random matrix with normalized columns. Finally, the number of Monte Carlo trials was chosen as 1000.

B. 1D CESS

In Fig. 4 the detection rates P_D and the false alarm rates P_F for different methods are illustrated as a function of the compression κ. Above $\kappa = 15\%$, LS, CS and 1D CESS all show perfect reconstruction. Below 15%, LS has a higher detection rate than CS, but vastly more false alarms. In contrast, 1D CESS begins to deteriorate significantly at a very low compression ratio of 6%. In the chosen test setup the number of non-zero elements is reduced from 40 spectral points to $J = 5$ edges. Thus, the reconstruction quality is adequate even at the minimal compression ratio $\kappa = 6/100 > J/N = 5/100$ which offers unique reconstruction. Furthermore, this leads to reduced complexity in terms of OMP iterations. Altogether, it

ISBN 978-90-827970-1-5 © EURASIP 2018

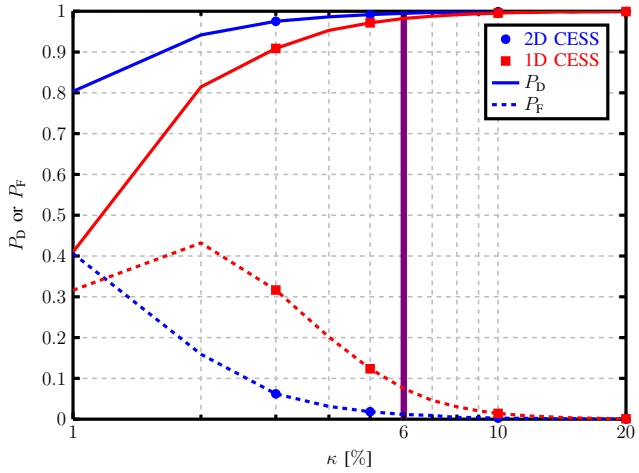

Fig. 5. Detection and false alarm rates of 2D and 1D CESS for $K = 20$ time instances versus compression κ.

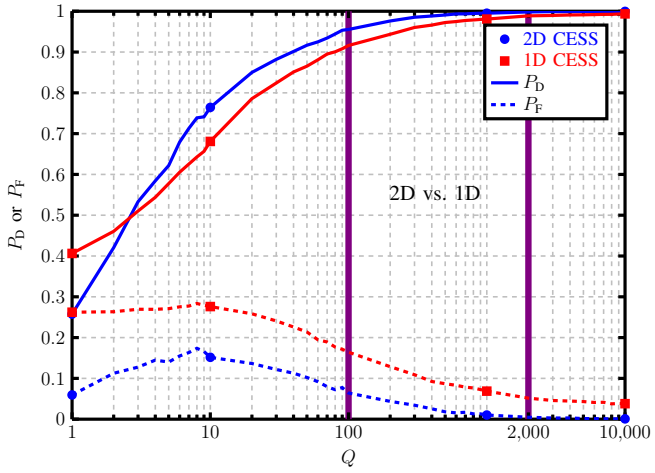

Fig. 6. Detection and false alarm rates of 2D and 1D CESS for $K = 20$ time instances as a function of frames Q. Fixed $\eta_{\text{WED}} = 1.5$ and $\kappa = 6\%$.

TABLE II
NMSE OF 2D AND 1D CESS FOR $K = 20$ TIME INSTANCES AND κ.

κ [%]	3	6	10	20
2D CESS [dB]	−13.56	−20.73	−25.19	−30.26
1D CESS [dB]	−5.27	−12.57	−18.49	−27.44

can be clearly seen that 1D CESS outperforms the other two approaches in the test setup.

C. 2D CESS

The performance of the spectral estimator in terms of detection and false alarm rates when using 2D CESS and $K = 20$ can be deduced from Fig. 5. In comparison to 1D CESS, slightly higher detection rates are achieved for relevant compression up to 3% whereas false alarms can be significantly reduced at least by half, e.g., from 7.5% to 1% at $\kappa = 6\%$. Another measure for comparing the performance regarding reconstruction accuracy is the normalized Mean Square Error (nMSE) which is related to the ideal spectrum and given for some values of κ in table II. It can be clearly seen that 2D CESS achieves an at least 3 dB smaller nMSE for relevant compression than 1D CESS. In summary, it can be stated that in accordance with the first guess 2D CESS offers performance benefits because it utilizes the additional structural information in the time domain. However, 2D CESS introduces a delay due to the longer time window $T = K\Delta t$. For a delay oriented comparison, we fixed the threshold to $\eta_{\text{WED}} = 1.5$ and depicted Q in Fig. 6. We can see that at lower Q mainly false alarm performance is better for 2D CESS. As a result, Q can be reduced, e.g., by a factor of $K = 20$ from 2000 to 100 for constant $P_F \approx 5\%$, in comparison to 1D CESS. Hence, both 2D and 1D CESS can have the same sampling time at a comparable false alarm rate. But this does not hold for detection rates: A reduction by $K \approx 6.7$ from 2000 to 300 is possible here. In conclusion, 2D CESS introduces a delay and additionally has a higher computational complexity.

VI. CONCLUSION

The main results of called work can be summarized as follows: 1D CESS can provide a lower compression ratio than the CS and LS approach due to exploitation of the inherent signal structure. Good performance can be achieved until the actual edge spectrum occupation of 5% is reached. 2D CESS allows for an even better performance if time-domain edges are exploited. Therefore, we assume CESS to be a proper candidate for future CR and CM applications.

ACKNOWLEDGMENT

This research has been funded by the Federal Ministry for Economic Affairs and Energy of Germany through the AiF in the project KoMe (project number 18350 BG/2).

REFERENCES

[1] E. Axell, G. Leus, E. G. Larsson, and H. V. Poor, "Spectrum Sensing for Cognitive Radio [State-of-the-art and recent advances]," *IEEE Signal Processing Magazine*, vol. 29, no. 3, pp. 101–116, May 2012.

[2] T. Yücek and H. Arslan, "A Survey of Spectrum Sensing Algorithms for Cognitive Radio Applications," *IEEE Communications Surveys & Tutorials*, vol. 11, no. 1, pp. 116–130, Mar. 2009.

[3] "IEEE Standard for Information technology–Telecommunications and information exchange between systems – Local and metropolitan area networks – Specific requirements – Part 19: TV White Space Coexistence Methods," *IEEE Std 802.19.1-2014*, pp. 1–326, Jun. 2014.

[4] Z. Tian and G. B. Giannakis, "Compressed Sensing for Wideband Cognitive Radios," in *IEEE International Conference on Acoustics, Speech and Signal Processing (ICASSP)*, Apr. 2007, pp. 1357–1360.

[5] D. Cohen and Y. C. Eldar, "Sub-Nyquist Sampling for Power Spectrum Sensing in Cognitive Radios: A Unified Approach," *IEEE Transactions on Signal Processing*, vol. 62, no. 15, pp. 3897–3910, Aug. 2014.

[6] D. Cohen and Y. C. Eldar, "Sub-Nyquist Cyclostationary Detection for Cognitive Radio," *IEEE Transactions on Signal Processing*, vol. 65, no. 11, pp. 3004–3019, Jun. 2017.

[7] Y. C. Eldar and G. Kutyniok, *Compressed Sensing - Theory and Applications*. Cambridge University Press, 2012.

[8] Y. L. Polo, Y. Wang, A. Pandharipande, and G. Leus, "Compressive Wideband Spectrum Sensing," in *IEEE International Conference on Acoustics, Speech and Signal Processing (ICASSP)*, Apr. 2009, pp. 2337–2340.

[9] M. Grant and S. Boyd, "CVX: Matlab Software for Disciplined Convex Programming, version 2.1," http://cvxr.com/cvx, Dec. 2017.